

Effect of Viewing Angle on the Infrared Brightness Temperature of Snow

JEFF DOZIER

Department of Geography, University of California, Santa Barbara, California 93106

STEPHEN G. WARREN

Department of Atmospheric Sciences, University of Washington, Seattle, Washington 98195

Remote sensing of snowpack temperatures from satellites requires knowledge of the spectral emissivity of snow. A model for spectral emissivity is combined with the Planck function to calculate brightness temperature of snow in thermal infrared wavelengths for a range of grain sizes and viewing angles. Emissivity variations caused by density, grain shape, liquid water, and grain size are apparently unimportant, but emissivity varies with viewing angle to produce differences between thermodynamic temperature and brightness temperature as large as 3 K at wavelengths 12 to 14 μm , within the major atmospheric infrared window. This difference is also verified by experimental measurements. An equation to convert brightness temperatures to thermodynamic temperatures is presented, and this is also combined with a dual-wavelength atmospheric correction method. The spectral emissivity model is also used to calculate an 'all-wave' emissivity of snow: 0.985-0.990 for all grain sizes.

INTRODUCTION

Infrared radiance measurements from satellites or from portable field instruments can be used for remote estimation of snow surface temperature. These temperatures could in turn be used to calibrate a snow surface energy budget model [e.g., Anderson, 1976] over a drainage basin or to map snow cover at subpixel resolution [Wan, 1981]. For such purposes, however, the radiance measurements must be corrected for variations in the emissivity of snow and also for atmospheric attenuation. Here we discuss the forms of these two corrections. We show that while variations in emissivity because of grain size, density, or liquid water are apparently not significant in the wavelengths of the atmospheric water vapor windows, the effect of viewing angle must be considered, especially in mountainous areas, where local slope combined with satellite scan angle can lead to large viewing (nadir) angles. Emissivity variations with viewing angle must also exist for other surfaces because reflectance usually increases significantly with incidence angle.

THEORETICAL MODEL FOR SNOW EMISSIVITY

From the principle of detailed balance, the probability for spectral emission of radiation in a given direction is equal to the probability of absorption of radiation at that same wavelength if it were incident along that same direction. This is a consequence of time-reversal symmetry: the probability of occurrence of a process is equal to the probability of occurrence of the reverse process [Reif, 1965]. Applied to thermal radiation, this principle is known as Kirchhoff's law [Siegel and Howell, 1981]. For an opaque or 'semi-infinite' medium, radiation can only be reflected or absorbed, hence for any incident or viewing direction angle, directional emissivity (also called emittance) can be calculated if the directional-hemispherical reflectance (the term defined by Nicodemus et al. [1977] for total hemispherical reflectance of direct irradiance) is known:

$$\varepsilon_s(\lambda, \mu_v) = 1 - R_s(\lambda, \mu_v) \quad (1)$$

Here $R_s(\lambda, \mu_v)$ is the directional-hemispherical reflectance, neglecting polarization, for wavelength λ at incidence angle $\vartheta_v = \arccos \mu_v$, and $\varepsilon_s(\lambda, \mu_v)$ is the directional emissivity for the same viewing angle; ϑ_v is the angle from vertical, $\vartheta_v = 0$ for normal viewing. This equation assumes azimuthal symmetry, so that ε_s depends only on the angle between the local normal and the direction of emission. We neglect polarization as probably unimportant. Hansen [1971] compared the intensities obtained in the case in which polarization is correctly accounted for and in the scalar approximation in which polarization is neglected, in his multiple scattering computations of clouds, for the visible wavelength region. He found that the difference in intensities between considering and not considering polarization was generally less than 1%. Moreover, the instruments used to measure thermal emission usually do not have polarizing filters.

Because ice has such strong absorption in the infrared wavelengths, snow is infinitely thick at small depths as far as emission and absorption of infrared radiation are concerned. The underlying surface does not contribute to thermal emission, even for snow only a few millimeters thick, so here we need not consider transmission and may use the simpler formulas appropriate to a semiinfinite scattering medium. The equation for directional emissivity $\varepsilon_s(\lambda, \mu_v)$ is derived by applying (1) to the equation for directional-hemispherical reflectance in Wiscombe and Warren [1980], which was derived from the delta-Eddington approximation to the equation of radiative transfer

$$\varepsilon_s(\lambda, \mu_v) = \frac{\xi \mu_v [\omega^* b^* + 1 + P] + 1 + P - \omega^*}{(1 + P)(1 + \xi \mu_v)} \quad (2)$$

Hemispherically averaged emissivity $\varepsilon_d(\lambda)$ is derived by integrating directional emissivity over the hemisphere:

$$\varepsilon_d(\lambda) = 2 \int_0^1 \mu_v \varepsilon_s(\lambda, \mu_v) d\mu_v$$

$$= \frac{(2b^* + 2)\omega^* \ln(\xi + 1) + \xi[(\omega^* b^* + 1 + P)\xi - \omega^*(2b^* + 2)]}{\xi^2(1 + P)} \quad (3)$$

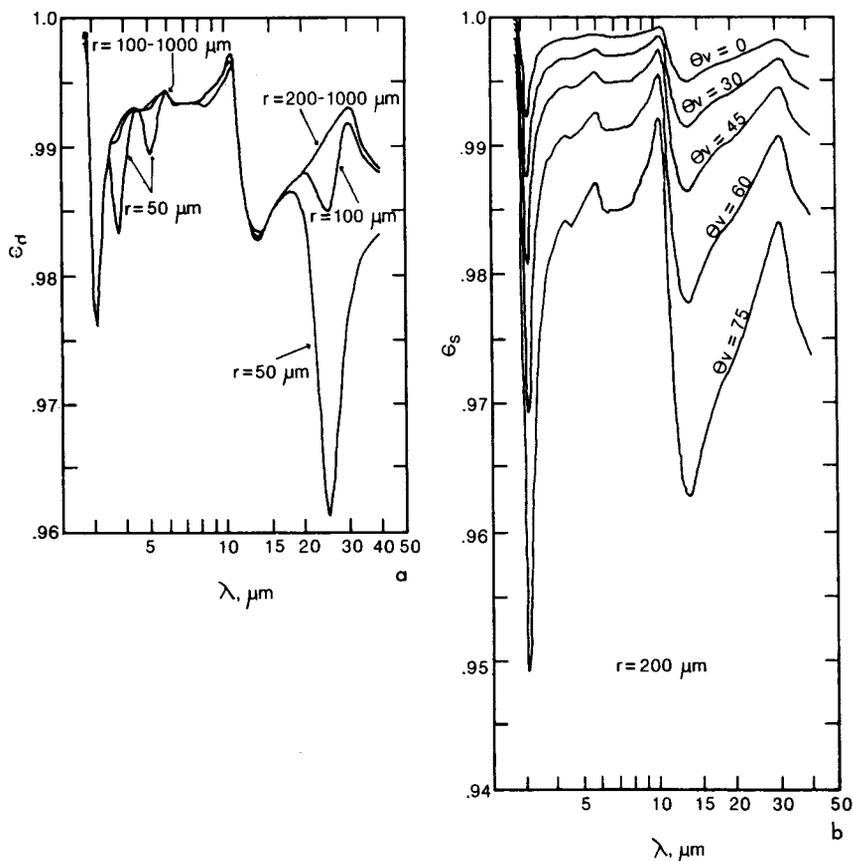


Fig. 1. (a) Hemispherically averaged emissivity of snow $\epsilon_d(\lambda)$ for grain radii from 50 to 1000 μm . (b) Directional emissivity of snow $\epsilon_s(\lambda, \mu_v)$ for grain size $r = 200 \mu\text{m}$ for viewing angles θ_v from 0 to 75°.

The other variables in (2) and (3) are

$$g^* = \frac{g}{1 + g}$$

$$\omega^* = \frac{(1 - g^2)\omega}{1 - g^2\omega}$$

$$b^* = \frac{g^*}{1 - \omega^*g^*}$$

$$\xi = [3(1 - \omega^*g^*)(1 - \omega^*)]^{1/2}$$

$$P = \frac{2\xi}{3(1 - \omega^*g^*)}$$

The single scattering albedo ω and asymmetry factor g in the scattering phase function are calculated from the Mie equations and depend on the complex refractive index of ice and the snow grain size, represented by an optically equivalent sphere of radius r ; ω is the total fraction of the radiation intercepted by a snow grain that is scattered (instead of absorbed), and g is the mean value of the cosine of the scattering angle. Thus $0 \leq \omega \leq 1$ and $-1 \leq g \leq 1$; $g = 0$ for isotropic scattering, $+1$ for completely forward scattering, and -1 for backward scattering; ω^* and g^* are the delta-Eddington transformations of ω and g [Joseph *et al.*, 1976].

The justification for modeling irregularly shaped snow grains as a collection of spheres is considered later in this

paper, using an equivalent spherical radius to mimic the scattering properties. Rapid methods for Mie calculations are described by Wiscombe [1980] and Nussenzveig and Wiscombe [1980]. For the complex refractive index m of ice in the range $2.8 \leq \lambda \leq 33 \mu\text{m}$, we use the measurements of Schaaf and Williams [1973], beyond $33 \mu\text{m}$, we apply temperature corrections to the measurements made by Bertie *et al.* [1969] at 100 K.

In Figure 1 we show calculations of the spectral emissivity of snow, averaged over emission angle, for four grain sizes and for a single grain size $r = 200 \mu\text{m}$ at five emission angles. These are consistent with the emissivity calculations for $\lambda \leq 12 \mu\text{m}$ in Figures 8b and 11b of Wiscombe and Warren [1980]. The optically equivalent sphere (assuming such an equivalence can be made) is likely to be that which has the same volume-to-surface ratio as the real nonspherical snow particle [Warren, 1982]. This means that the equivalent sphere for a stellar crystal would have a diameter comparable to the width of a stellar branch. The smallest grain size considered here, $r = 50 \mu\text{m}$, is the smallest effective spherical radius required by Wiscombe and Warren to match the highest measured reflectance values in the solar near-infrared wavelengths. Such fine grains represent the finest sizes of any significant fraction in Antarctic drift snow; snow in the mid-latitudes typically has $r \geq 50 \mu\text{m}$ when newly fallen, increasing with age to $r \sim 1 \text{ mm}$ for old melting snow.

The emissivity is sensitive to grain size only at certain wavelengths. In particular, it is insensitive in the atmospheric water vapor window from 8 to 14 μm , where most of the emitted radiation is concentrated, but it is somewhat sensi-

tive in the 3.5–4.0 μm water vapor window, especially for small grains. There is little radiation emitted from the earth in the short wavelengths of the Planck function (less than 0.1% for $\lambda < 4 \mu\text{m}$ at $T = 270 \text{ K}$) so these variations are not of interest for energy budget studies. They are of interest for remote sensing, however, because the clearest atmospheric water vapor window in the infrared is from 3.5–4.0 μm , where channel 3 on the Advanced Very High Resolution Radiometer (AVHRR) on the NOAA Tiros-N series satellites is located. The variation of emissivity with viewing angle at wavelengths 8 to 14 μm is of the most practical importance: for remote sensing because these wavelengths are within the major water vapor window and for energy budget purposes because the Planck blackbody function peaks between 10 and 11 μm for typical snow surface temperatures. From 20 to 40 μm emissivity is highly sensitive to view angle and to grain size for $r < 200 \mu\text{m}$, but atmospheric absorption in these wavelengths is almost complete.

RELATIONS BETWEEN EMISSIVITY AND BRIGHTNESS TEMPERATURE

Emitted spectral radiance L at wavelength λ in direction μ_ν from a surface at thermodynamic temperature T is given by multiplying the directional emissivity by the Planck function β :

$$L(\lambda, \mu_\nu) = \epsilon_s(\lambda, \mu_\nu)\beta(\lambda, T) \quad (4)$$

where

$$\beta(\lambda, T) = \frac{2hc^2\lambda^{-5}}{e^{hc/(k\lambda T)} - 1} \quad (5)$$

$h = 6.63 \times 10^{-34} \text{ Js}$ is Planck's constant, $c = 3 \times 10^8 \text{ m/s}$ is the velocity of light, and $k = 1.38 \times 10^{-23} \text{ J/K}$ is Boltzmann's constant. For the dimensions to be correct, λ must be in meters.

Monochromatic brightness temperature T_B can be found by solving the Planck function for T , given the emitted radiance. The brightness temperature for a given wavelength is thus the temperature of a blackbody that emits the same amount of radiation at that wavelength as does the snow. The following equations give the relationship between T_B , T , and ϵ :

$$T_B(\lambda, \mu_\nu) = \frac{hc}{k\lambda \ln \left[\frac{e^{hc/(k\lambda T)} + \epsilon - 1}{\epsilon} \right]} \quad (6)$$

$$T = \frac{hc}{k\lambda \ln [1 + \epsilon e^{hc/(k\lambda T_B)} - \epsilon]} \quad (7)$$

Note that if $\epsilon = 1$, each of these equations reduces to the identity $T_B = T$. Otherwise, the error introduced if one were to assume snow to be a black body is $T_B - T$; this error is dependent on wavelength, even for a constant emissivity, as Figure 2 shows. Within the range of snow temperatures commonly encountered in the mid-latitudes (250–273 K), the quantity $T_B - T$ is rather insensitive to T for $\epsilon \geq 0.98$.

OTHER FACTORS POSSIBLY AFFECTING SNOW EMISSIVITY

Of all the snowpack parameters that affect snow albedo or emissivity in various regions of the electromagnetic spec-

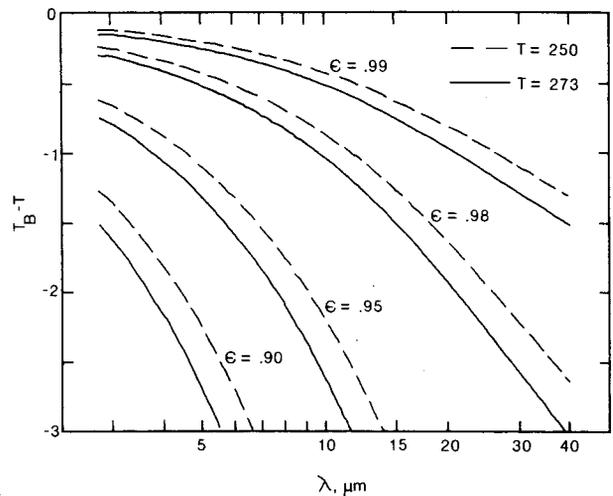


Fig. 2. Spectral variation of difference between brightness and thermodynamic temperatures $T_B - T$ for emissivities from 0.90 to 0.99 and temperatures 250 and 273 K.

trum, it turns out that only the emission angle has a significant influence in the thermal infrared. Because of the strong absorption by ice through the infrared, as noted above, a snowpack need only be a few millimeters thick to obscure any effect of the underlying surface. Thus we may say that emissivity is unaffected by snowpack thickness. Again, because of the strong absorption, trace amounts of impurities cannot affect snow infrared emissivity (even though they may affect solar albedo). There remain three parameters that cannot yet be ruled out as influencing infrared emissivity: namely, grain shape, snow density, and liquid water content, and we consider these in turn. We conclude that they are probably all negligible, as follows.

Nonsphericity of Snow Grains

Snow particles occur in a variety of shapes, many of them not only nonspherical but concave as well [see *Perla and Martinelli*, 1978]. To model them via Mie scattering theory therefore demands the assumption that the scattering properties of the grains can be appropriately mimicked by an 'equivalent sphere' of known radius. Some proposed equivalences are the sphere of equal volume, equal projected area, equal surface area, or equal volume/surface ratio.

Experimental and theoretical comparisons of scattering by ensembles of nonspherical particles with scattering by equivalent spheres (with the definition of 'equivalent' chosen from the candidates listed above) generally show that the extinction, absorption, and scattering efficiencies are about the same, especially when averaged over orientation and size. However, the details of the scattering phase function are sensitive to nonsphericity. The largest differences occur for side- and backscattering (i.e., scattering angles $>90^\circ$ from the forward direction); measurements usually show that sidescattering is enhanced by nonsphericity while backscattering is reduced, but the opposite may be the case for absorbing, highly concave particles [Zerull *et al.*, 1979]. The calculations of *Mugnai and Wiscombe* [1980] also show that while sidescattering is usually increased and backscattering is reduced, there are some exceptions for only moderately nonspherical particles with refractive indices similar to those of ice in the infrared. Both measurements and theoretical

calculations apparently show that forward scattering from nonspherical particles matches Mie theory well.

To evaluate the effect of nonsphericity on our delta-Eddington model of snow emissivity, we need to examine the variations in single scattering albedo ω and asymmetry factor g with particle size and shape. Unfortunately the calculations in the literature [Mugnai and Wiscombe, 1980; Pollack and Cuzzi, 1980] do not cover the full Mie size or refractive index ranges appropriate to snow. Both papers are restricted to Mie parameters $x \leq 10$ (whereas $x \sim 100$ for snow at $\lambda = 10 \mu\text{m}$), and both consider m_{re} only in the range 1.5–1.7, slightly higher than the real refractive index of ice in the wavelengths of the atmospheric water vapor windows. Mugnai and Wiscombe consider a range for m_{im} from nonabsorbing to highly absorbing, but Pollack and Cuzzi restrict their calculations to only nonabsorbing and slightly absorbing particles.

Because absorption and scattering efficiencies are not much affected by particle shape, single scattering albedo ω is also not much affected. In the size ranges considered by Mugnai and Wiscombe and Pollack and Cuzzi, asymmetry factor g decreased as a result of nonsphericity. In their ranges of sizes and refractive indices, however, g is also sensitive to particle size, whereas in the size ranges appropriate for our problem, wavelengths 3–15 μm and snow grain radii 50–2000 μm , g is insensitive to size. Thus nonsphericity corrections are probably small, although we cannot definitively calculate their magnitude. The exception might occur in a case where the grains were not only nonspherical but oriented as well, because the effects of shape are then not averaged over orientation.

Density

Because snow particles are closely packed, they may be in each other's 'near field,' meaning that Mie scattering theory is inapplicable. Wiscombe and Warren reviewed the possible effects and pointed out that interparticle interference should be neglected for particles whose center-to-center separation d is large in comparison to the wavelength λ . Since $d \gg \lambda$ in the solar spectrum, no interference should be observed, and this is confirmed by Bohren and Bescht's [1979] observation that the albedo of a thick snowpack is independent of density. For the thermal infrared spectrum, where for fine-grain snow, d is only 5 to 10 times λ , interference effects may arise, making snow thermal emissivity a function of density as well as grain size.

It is possible to estimate the effect, using the adjustments to Mie theory that Gate [1973] made to investigate the dependence of reflectance and transmittance on density in thick colloidal suspensions of latex in water. Gate modified the relative index of refraction—the refractive index of the grains relative to that of the surrounding medium—by imagining a fictitious 'medium' whose optical properties lie somewhere between those of the particles themselves and the fluid in which they are embedded (water in Gate's case, air in ours). Applied to the problem of snow, his equation for the relative index of refraction (which is what controls the radiation scattering properties) is

$$m_{\text{re}} = \frac{m_{\text{re}}^{(\text{ice})}}{m_{\text{re}}^{(\text{med})}} \quad (8)$$

The 'medium' is a mixture of air and ice, so that the

refractive index contrast between ice and the medium is less than that between ice and air. The optical properties of the air have to be modified because of the presence of ice of volume V_{ice} in the 'near field.' The index of refraction of this mixture is

$$m_{\text{re}}^{(\text{med})} = (1 - V_{\text{ice}})m_{\text{re}}^{(\text{air})} + V_{\text{ice}} m_{\text{re}}^{(\text{ice})} \quad (9)$$

where $m_{\text{re}}^{(\text{air})} = 1$. Warren [1982, Figure 4] suggests that the near field should be taken to be a shell, one or a few wavelengths thick, surrounding the particle. He uses several empirical schemes, based on the packing of snow grains, to estimate a value for V_{ice} within a shell 1 wavelength thick surrounding the particle; this value is a function of snow density and size parameter. Some sample calculations illustrate typical correction magnitudes: At $\lambda = 10 \mu\text{m}$, $m_{\text{re}}^{(\text{ice})} = 1.197$. For snow of radius $r = 200 \mu\text{m}$ and density $\rho = 450 \text{ kg/m}^3$, $V_{\text{ice}} = 0.0189$, calculated by Warren's method. From (9), $m_{\text{re}}^{(\text{med})} = 1.004$, and from (8) the index of refraction of the snow $m_{\text{re}} = 1.193$. If ρ is increased to 600 kg/m^3 , $V_{\text{ice}} = 0.0682$, $m_{\text{re}}^{(\text{med})}$ rises to 1.013, and m_{re} drops to 1.181. It is also necessary to adjust the Mie size parameter x :

$$x = m_{\text{re}}^{(\text{med})} \frac{2\pi r}{\lambda} \quad (10)$$

where λ is wavelength in vacuum.

To make this near-field adjustment a truly consistent formulation that gives the correct emissivity in both limits $x \ll 1$ and $x \gg 1$, one would have to adjust the complex refractive index, treat the medium of ice and air as absorptive, and account for Fresnel reflection by the medium at the snow surface. There is also some question as to whether Gate's mixing rule is the appropriate one, i.e., whether instead of refractive index, one should average dielectric constants. We do not include these embellishments here because we just wish to show that the magnitude of the effect of density on emissivity is negligibly small. By adjusting only m_{re} , we should get a good approximation to the true near-field effects.

Figure 3 shows calculations of the hemispherical emissivity of snow incorporating near-field calculations. On this figure, emissivity is shown for wavelengths as long as 150 μm , not because there is much thermal emission at 150 μm but just to show how far one must go in wavelength before one notices a significant effect of near-field interference. Near-field effects are unlikely to be important for $\lambda < 50 \mu\text{m}$ (i.e., for 96% of the thermal emission at $T = 270 \text{ K}$), for any combination of density and grain size. Part of the reason for this is the decrease in the refractive index of ice between $\lambda = 15 \mu\text{m}$ and $\lambda = 45 \mu\text{m}$. While more and more ice is in the near field as wavelength increases, ice refractive index becomes closer to unity, so that it is altered little when the near-field correction is applied. Furthermore, high densities (450–650 kg/m^3) are normally associated with large grain sizes. Near-field effects at wavelengths longer than 50 μm are insignificant because of the small amount of energy emitted.

Liquid Water

In some wavelengths the refractive index of water [Hale and Querry, 1973] varies significantly from that of ice [Schaaf and Williams, 1973]. For wavelengths between 13 and 17 μm the real refractive index of ice is greater than that of water, while for $\lambda > 25 \mu\text{m}$ the refractive index of water is

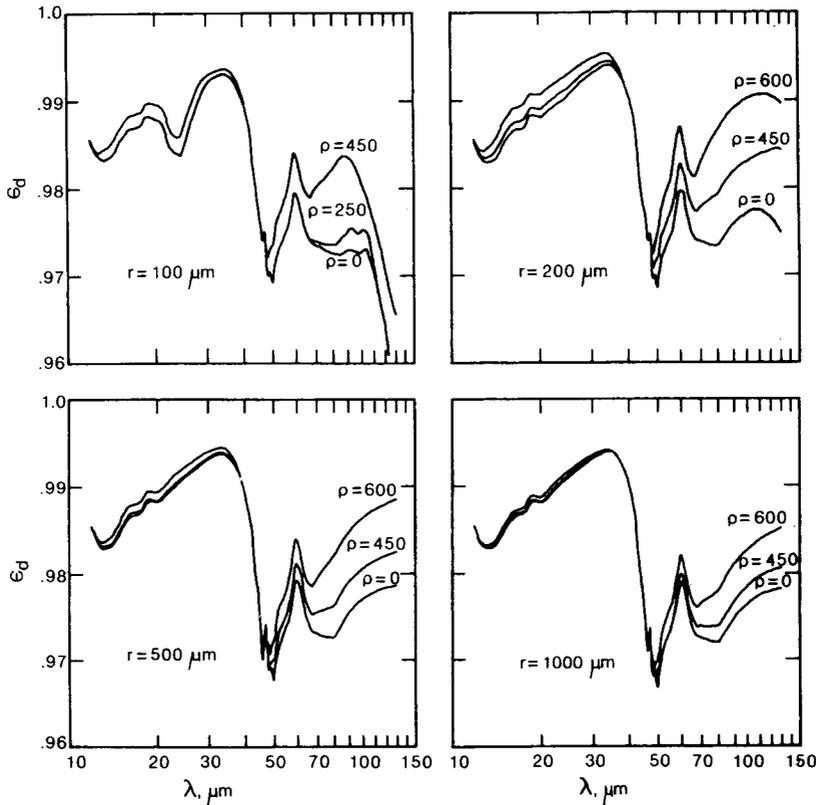


Fig. 3. Near-field effects on hemispherical emissivity of snow. Grain sizes r from 100 to 1000 μm are shown, as well as snow densities ρ from 0 to 600 kg/m^3 . Density $\rho = 0$ corresponds to the absence of any near-field effect.

greater. For $17 \leq \lambda \leq 40 \mu\text{m}$ the imaginary part of the refractive index of water is greater, i.e., water is more absorptive than ice. To adjust for liquid water in the snow-pack, we compute weighted averages for the Mie asymmetry parameter g and single scattering albedo ω :

$$\bar{g} = \frac{S_{\text{ice}} Q_{\text{sca}}^{(\text{ice})} g^{(\text{ice})} + S_{\text{water}} Q_{\text{sca}}^{(\text{water})} g^{(\text{water})}}{S_{\text{ice}} Q_{\text{sca}}^{(\text{ice})} + S_{\text{water}} Q_{\text{sca}}^{(\text{water})}} \quad (11)$$

$$\bar{Q}_{\text{ext}} = \frac{S_{\text{ice}} Q_{\text{ext}}^{(\text{ice})} + S_{\text{water}} Q_{\text{ext}}^{(\text{water})}}{S_{\text{ice}} + S_{\text{water}}} \quad (12)$$

$$\bar{Q}_{\text{sca}} = \frac{S_{\text{ice}} Q_{\text{sca}}^{(\text{ice})} + S_{\text{water}} Q_{\text{sca}}^{(\text{water})}}{S_{\text{ice}} + S_{\text{water}}} \quad (13)$$

$$\bar{\omega} = \bar{Q}_{\text{sca}} / \bar{Q}_{\text{ext}} \quad (14)$$

Q_{sca} and Q_{ext} are the scattering and extinction efficiencies, respectively; S_{ice} and S_{water} are the respective geometric cross sections of ice and water.

If both ice and water existed as separate spheres, the geometric cross sections would be related to the volume fractions by

$$\frac{V}{S} = \frac{\sum r^3}{3 \sum r^2} \quad (15)$$

where the sums are over the range of particle radii in the size distribution. Unfortunately, the geometry of water in grain clusters in wet snow is not well known. Colbeck's [1982] photographs indicate that most of the water is held in veins within three- or four-grain clusters and that the air-ice

surface area is much greater than the air-water surface area. Thus the likely effect of the ice-water geometry is to shield the water. Therefore, if we assume, for simplicity, that the ice and water exist as separate, spherical particles, we will overestimate the effect of the liquid water on snow emissivity. Since our aim here is only to show that the magnitude of the liquid water effect is entirely negligible, we follow this approach. We assume that the water 'particles' are the same size as the ice grains, so the S 's in (11–13) may be replaced by the volume fractions.

We caution against using this approach for microwave frequencies. For wavelengths where there is an enormous difference between the refractive indices of ice and water, a model would have to consider more precisely the geometry of the water inclusions.

Figure 4 shows hemispherical emissivity for grain sizes $r = 50 \mu\text{m}$ and $r = 100 \mu\text{m}$; for a high water content: 20% of the total particle volume, with the remaining 80% ice. For $r > 100 \mu\text{m}$ the results do not change significantly from the $r = 100 \mu\text{m}$ case. Such a high water content would only occur with surface melting of low-density, fine-grain snow. Normally in melting, draining, coarse-grain snow, maximum free-water content is 8–10%. The reason we use the 20% value in our calculations is to show that even this unrealistic amount of liquid water has an insignificant effect on snow emissivity.

EFFECT OF VIEWING ANGLE ON SNOW BRIGHTNESS TEMPERATURE

In Figure 5 we combine the results of our calculations of snow emissivity and the relationship between emissivity, wavelength, and brightness temperature, to show values of

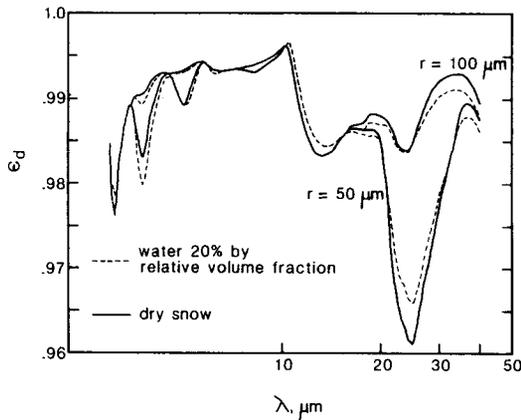


Fig. 4. Effect of liquid water on hemispherical emissivity of snow. Grain radii 50 and 100 μm are shown, both fine-grain sizes. For larger grain sizes the variation from the dry snow case is even smaller. Even a high water content, 20% by relative solid volume fraction, has insignificant effect.

$T_B - T$ for snow, for grain size $r = 200 \mu\text{m}$ at viewing angles $0^\circ, 30^\circ, 45^\circ, 60^\circ,$ and 75° . Because $T_B - T$ is dependent on both emissivity and wavelength, the low emissivity values at $\lambda \sim 3 \mu\text{m}$ do not cause as great a drop in brightness temperature as those at $\lambda > 12 \mu\text{m}$. The large differences between T_B and T at wavelengths 12–14 μm are significant because this wavelength region is within the 8–14 μm atmospheric water vapor window. For 20–40 μm the difference $T_B - T$ is also sensitive to grain size for $r < 200 \mu\text{m}$, but this is not so significant because atmospheric absorption in these wavelengths is almost complete, and they are not commonly used for sensors.

The possibilities of measurement error with instruments used for remote sensing of surface temperature are investigated by integrating the results in Figure 5 over the wavelength ranges and response functions of some common sensors. Here the equation for wavelength-integrated T_B is more complicated, although the definition is the same—the temperature of a blackbody that emits the same amount of wavelength-integrated radiation as the snow. For a given sensor with response $\Phi(\lambda)$ within some interval $[\lambda_1, \lambda_2]$ and

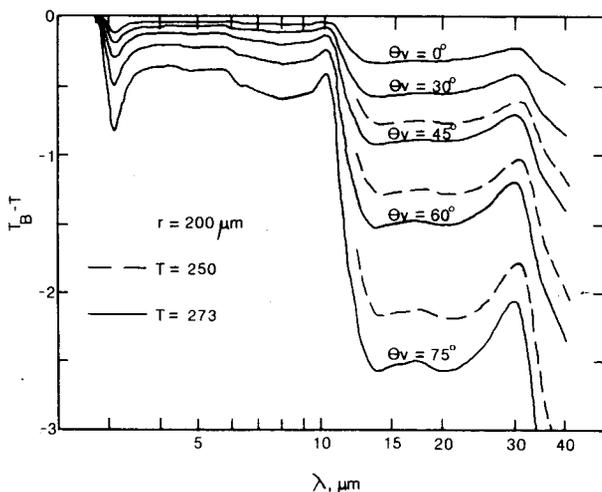


Fig. 5. Spectral variation of $T_B - T$ for snow of temperature $T = 273 \text{ K}$ and grain size $r = 200 \mu\text{m}$, for viewing angles 0° to 75° . For $\theta_v \geq 45^\circ$ and $\lambda \geq 12 \mu\text{m}$, values of $T_B - T$ for $T = 250 \text{ K}$ are also shown.

TABLE 1. Infrared Sensor Wavelengths Considered

Sensor	Wavelength Range μm
NOAA 7 channel 3	3.53–3.94
NOAA 7 channel 4	10.32–11.36
NOAA 7 channel 5	11.45–12.42
Barnes PRT-5 radiometer	9.5–11.5
Telatemp radiant thermometer (or Barnes PRT-4 radiometer)	8–14
Eppley pyrgeometer	4–50

zero outside the interval, T_B is the root of

$$\int_{\lambda_1}^{\lambda_2} \Phi(\lambda) [\beta(\lambda, T_B) - \epsilon(\lambda)\beta(\lambda, T)] d\lambda = 0 \quad (16)$$

This relationship is considered for six sensors. Three of them are the thermal infrared channels of the AVHRR on the NOAA 7 polar-orbiting satellite, and the other three have the same wavelength ranges as instruments often used for field measurement of surface temperature. The Barnes PRT-5 and PRT-4 radiometers and the Telatemp infrared thermometer are hand-carried instruments used for spot measurements. The Eppley pyrgeometer is normally used to measure incoming longwave radiation at micrometeorological stations, but it can be pointed downward for surface temperature measurement. Except for the Eppley pyrgeometer, all these instruments have narrow fields of view, so that we need not integrate our results over a range of viewing angles. When the Eppley is used to measure surface temperature, its field of view is usually restricted by a tube whose temperature is also measured so that the radiation it emits can be compensated. Further details on the wavelength range of the instruments are given in Table 1. The filter response functions $\Phi(\lambda)$ for the three infrared channels on the NOAA 7 AVHRR are shown in Figure 6. For the three field instruments, $\Phi(\lambda)$ is assumed constant over the wavelength ranges in Table 1 and is therefore eliminated from (16).

In Figure 7 we show variations of $T_B - T$ with grain size and view angle for these sensors. The calculations show that the effect of grain size is only noticeable for fine-grain snow $r \sim 50 \mu\text{m}$, and only for NOAA 7 channel 3 and for the Eppley pyrgeometer. Even for these sensors the maximum

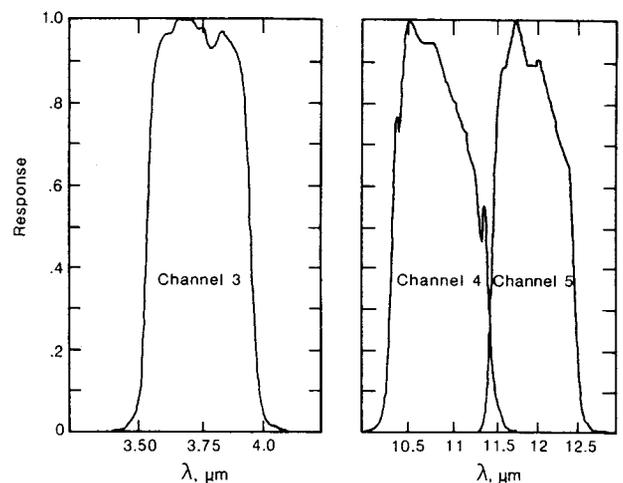


Fig. 6. Spectral response functions (normalized to maximum values) for channels 3–5 of the NOAA 7 AVHRR. Half-amplitude ranges are given in Table 1.

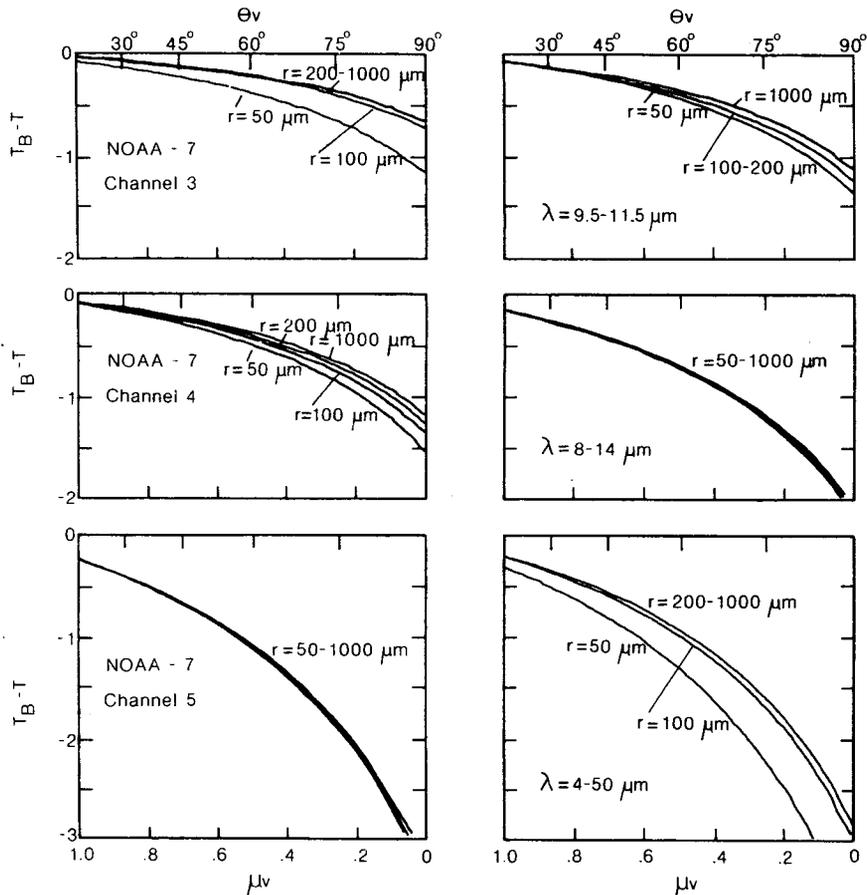


Fig. 7. Angular variation of $T_B - T$ for snow of temperature $T = 270$ K integrated over the wavelength ranges of the sensors listed in Table 1.

error because of grain size is about -0.5° . On the other hand, the viewing angle is significant, involving errors as large as -3° for NOAA 7 channel 5 and for the 8–14 and 4–50 μm sensors. Fortunately, however, since grain size is apparently unimportant, the curves in Figure 7 can be used to correct brightness temperature measurements with these instruments. Furthermore, (16) can be used to calculate corrections for other instruments with different response functions or different wavelength ranges.

For the six sensors listed in Table 1 we express the same information portrayed in Figure 7 as empirical correction equations. These were developed for 300- μm snow and would be accurate for all grain sizes above 100 μm , i.e., for all except fresh, newly fallen snow. They are expressed as rational Chebyshev approximations [Cody *et al.*, 1968] of the form

$$T_B - T = \frac{C_0 + C_1 \mu_v}{1 + D_1 \mu_v} \quad (17)$$

Values for the coefficients C_0 , C_1 , and D_1 are given in Table 2 for the six sensors in Table 1 and Figure 7. These can be used to convert brightness temperatures (at view angle $\arccos \mu_v$) to thermodynamic temperatures for any of the six sensors. If the brightness temperatures are measured from satellite, they must first be corrected for the intervening atmosphere.

Measurements made with a Telatemp radiant thermometer (8–14 μm) during February and May 1982 in the southern Sierra Nevada verify the general trend and magnitude of the

$T_B - T$ difference (Figure 8). The February measurements were made in the early morning over a smooth, wind-deposited snow surface consisting of broken stellar crystals about 0.5 mm across. Near-surface temperature, determined by thermocouple, was -20°C . The May measurements were made over a smooth snow surface that had been melting the previous day, although at the time of measurement the surface temperature was -3°C . The rounded crystals at the surface exceeded 1 mm across. The data agree with the model calculations for $\theta_v \leq 60^\circ$, but beyond this value they show a greater viewing angle dependence than the model. (The discrepancy may be somewhat worse than we show here, because in our calculation we have neglected reflection of infrared radiation by the snow. The radiant temperature of the sky becomes appreciable as we approach the 15 μm band of CO_2 absorption.)

There are three possible reasons for this discrepancy. One possibility is leakage in the instrument filter beyond 14 μm .

TABLE 2. Coefficients for Temperature Correction*

Sensor	C_0	C_1	D_1
NOAA 7 channel 3	-0.6719	0.5604	1.6817
NOAA 7 channel 4	-1.3117	1.1019	1.6805
NOAA 7 channel 5	-3.3526	2.7279	1.6266
Barnes PRT-5 radiometer	-1.2247	1.0292	1.6811
Telatemp radiant thermometer (or Barnes PRT-4 radiometer)	-2.1393	1.7513	1.6342
Eppley pyrgeometer	-2.8210	2.3105	1.6437

* Equation (21)

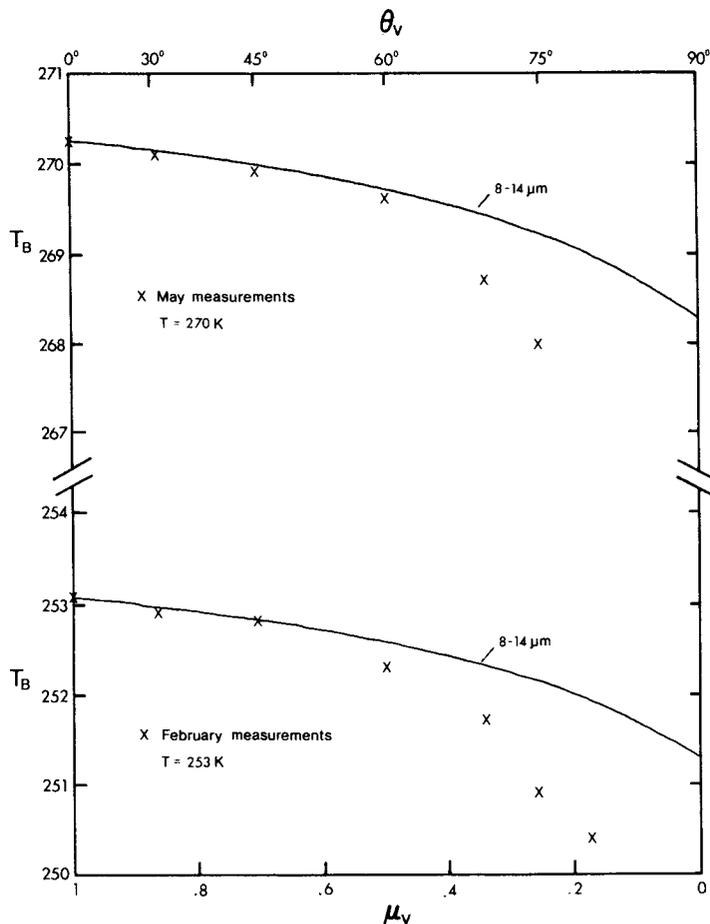


Fig. 8. Measurements vs. model calculations of the variation of brightness temperature with viewing angle for snow at thermodynamic temperatures -20°C (253 K) and -3°C (270 K). Measurements were made with a Telatemp radiant thermometer of wavelength range 8–14 μm .

The second possibility is nonsphericity of the surface grains. This could reduce the asymmetry factor g in the scattering phase function, increase the reflectance, and therefore decrease the emissivity. The third possibility is error in the delta-Eddington approximation itself. At large illumination angles, the delta-Eddington method underestimates reflectance, particularly at large optical depth [see Figure 3 of Joseph *et al.*, 1976]. This would lead to an overestimation of emissivity, which would reduce the $T_B - T$ difference.

We investigate this third possibility by comparing our delta-Eddington calculations to a doubling model, developed by Li [1982], for reflectance or emissivity of snow. Because the doubling model is computationally more expensive, we compare only for discrete wavelengths instead of wavelength-interval integrations. Figure 9 shows delta-Eddington and doubling calculations of snow emissivity as a function of viewing angle for grain size $r = 200 \mu\text{m}$ and wavelengths $\lambda = 10, 11, \text{ and } 12 \mu\text{m}$. The figure demonstrates that delta-Eddington and doubling calculations are close for $\mu_v \geq 0.25$ (i.e., $\theta_v \lesssim 75^{\circ}$) but diverge at greater viewing angles. The difference between delta-Eddington and doubling methods is enough to account for the measured discrepancy between theory and data in Figure 8.

ATMOSPHERIC CORRECTIONS

For clear atmospheres, a useful and generally successful method for correcting atmospheric effects over the ocean

surface uses multichannel infrared measurements. In the 10.5–12.5 μm window (NOAA 7 channels 4 and 5) the principal absorbing agent is water vapor, whereas at 3.5–4.0 μm , water vapor absorption is smaller, and absorption by nitrogen and other gases can be calculated. Therefore the

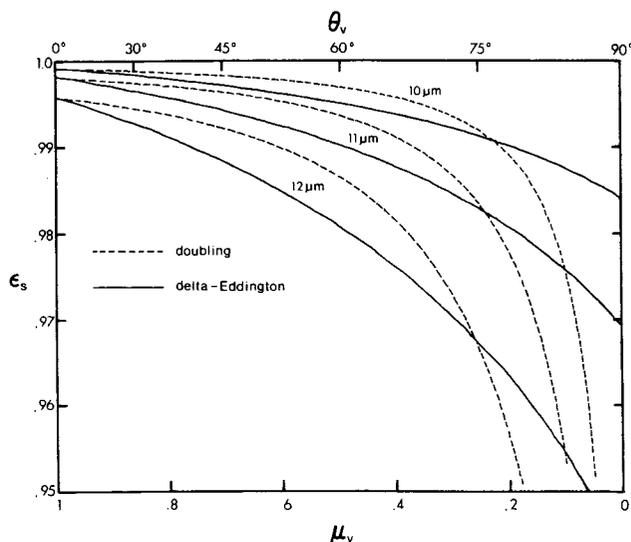


Fig. 9. Emissivity calculations by delta-Eddington and doubling methods for snow of size $r = 200 \mu\text{m}$ at three wavelengths, $\lambda = 10, 11, \text{ and } 12 \mu\text{m}$, as a function of viewing angle.

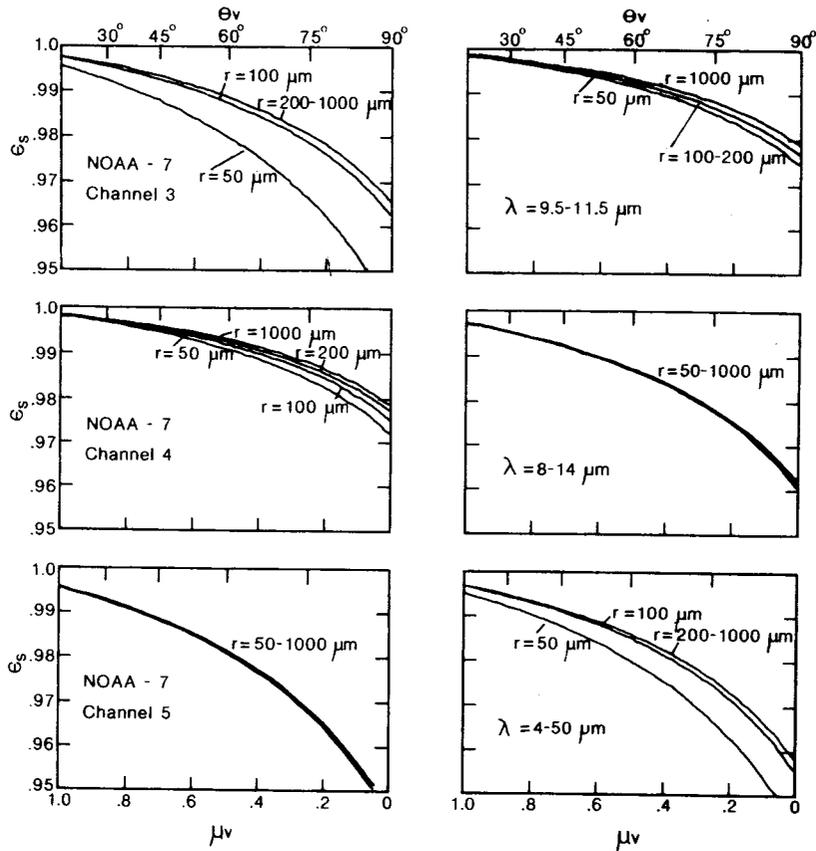


Fig. 10. Angular variation of emissivity for snow of temperature $T = 270$ K integrated over the wavelength ranges of the sensors listed in Table 1.

difference between the measurements in the two windows can be used to account for water vapor absorption and to determine the correct brightness temperature.

Anding and Kauth [1970], Prabhakara et al. [1973], Deschamps and Phulpin [1980], and McClain [1981] have developed and used this approach. An effective way to pursue it is to simulate brightness temperature differences for a variety of atmospheric temperature and humidity profiles by using a radiative transfer model to account for atmospheric absorption and emission and then using these simulations to develop empirical corrections. For a blackbody surface, McClain has proposed a correction of the form

$$T - T_4 = A(T_3 - T_4) + B \quad (18)$$

T_3 and T_4 are the space-measured brightness temperatures in NOAA AVHRR channels 3 and 4, and T is the surface temperature. Note that the blackbody assumption implies that at the surface $T_3 = T_4 = T$; A and B are coefficients determined from the numerical simulation; McClain calculated the values $A = 1.42$ and $B = 1.28$. The method has also been applied, but not yet extensively tested, on channels 4 and 5 instead of 3 and 4. These would allow use of the dual-channel method during daylight hours; reflection of solar irradiance in channel 3 sometimes contaminates the signal during the daytime.

To include our emissivity calculations in this atmospheric correction model, the right-hand side of (18) must be changed to add that portion of the $T_3 - T_4$ difference that results from emissivity variation with wavelength. Similarly, the left-hand side of (18) gives the brightness temperature difference between the surface and space and must be

modified for snow emissivity. These changes lead to the following equation, which should correct for both the atmosphere and snow emissivity:

$$T - T_4 = A \left[(T_3 - T_4) + \frac{C_0^{(3)} + C_1^{(3)} \mu_v}{1 + D_1^{(3)} \mu_v} \right] - (1 + A) \left[\frac{C_0^{(4)} + C_1^{(4)} \mu_v}{1 + D_1^{(4)} \mu_v} \right] + B \quad (19)$$

The superscripts on the C and D coefficients refer to AVHRR channels 3 and 4.

Frampton's [1982] data for satellite and surface temperature measurements in the southern Sierra Nevada show that the magnitude of the atmospheric correction at high altitude is usually small; uncorrected, space-measured temperatures at 10.5–11.5 μm from Tiros-N (a prototype for NOAA 7) were usually within 1.5 K of the surface-measured values when the field of view consisted entirely of snow.

A problem remaining to be solved for accurate snow-surface temperature measurements is the correction for subresolution-scale elements of different temperature than the snow. In the spring particularly, exposed rocks and trees may be much warmer than the snow, and the radiation emitted from these surfaces inflates the satellite-measured brightness temperatures, which on the NOAA-series satellite are averaged over pixels 1.1 km on a side. Dozier [1981] has shown that dual-channel thermal infrared measurements can be manipulated to solve for subpixel temperature fields, and Wan has combined the nonlinear equations for the subpixel problem with McClain's dual-channel atmospheric

correction algorithm. In this section we have shown how to combine the atmospheric correction algorithm with emissivity variations. A scheme for satellite temperature measurements incorporating all three elements—atmospheric corrections, emissivity variations, and subresolution temperature fields—has not been developed.

WAVELENGTH-INTEGRATED EMISSIVITY OF SNOW

In calculations of emitted longwave radiation within some wavelength interval it is often assumed that the surface is a 'grey' body with emissivity independent of wavelength. Such a wavelength-integrated emissivity is

$$\varepsilon = \frac{\int_{\lambda_1}^{\lambda_2} \varepsilon(\lambda)\beta(\lambda, T) d\lambda}{\int_{\lambda_1}^{\lambda_2} \beta(\lambda, T) d\lambda} \quad (20)$$

In Figure 10 we show the same information as in Figure 7, but expressed instead as apparent emissivities for the particular wavelength ranges, response functions, and viewing angles. Measurements have been reported in the literature for emissivities integrated over 8–14 μm for near-normal viewing angles, and Figure 10 supports the contentions of *Beutner and Kern* [1965] and *Griggs* [1968] that for this wavelength range and near-normal viewing angles, melting snow is almost a blackbody, with emissivities around 0.99.

In calculations of a snowpack energy budget it is necessary to include the longwave radiation emitted from the snow surface as a function of its temperature. This is usually calculated by the Stefan-Boltzmann equation $\varepsilon\sigma T^4$, where ε is an 'all-wave' emissivity and $\sigma = 5.67 \times 10^{-8} \text{ W m}^{-2} \text{ K}^{-4}$. Such an emissivity can be derived by integrating the emission from a snowpack over all wavelengths and angles:

$$\varepsilon = \frac{\pi}{\sigma T^4} \int_0^\infty \varepsilon_d(\lambda)\beta(\lambda, T) d\lambda \approx \frac{\int_3^{50\mu\text{m}} \varepsilon_d(\lambda)\beta(\lambda, T) d\lambda}{\int_3^{50\mu\text{m}} \beta(\lambda, T) d\lambda} \quad (21)$$

For grain size $r \geq 75 \mu\text{m}$ the hemispherically averaged all-wave emissivity of snow is between 0.988 and 0.990 for temperatures from 250–273 K. For fine-grain snow, $r = 50 \mu\text{m}$, the emissivity drops slightly to 0.985.

CONCLUSION

A recently developed model for the spectral albedo of snow, based on Mie scattering theory and the delta-Eddington approximation to the equation of radiative transfer, can be used to calculate directional and hemispherical spectral emissivities. Such calculations support the contention that in the infrared wavelengths snow is one of the blackest substances in nature; nevertheless, the variations in emissivity with viewing angle are not negligible. Within the 8–14 μm atmospheric water vapor window, failure to account for the effect of viewing angle could lead to temperature determination errors as large as 3 K. This magnitude is also verified by field measurements.

Since the thermal infrared emission does not depend on the (unknown) parameters of grain size, density, liquid water content, and impurity content but instead only on the

(known) viewing geometry, one may reliably use infrared emission of snow to obtain snow surface temperature, provided viewing geometry is accounted for. It is only the very top of the snowpack, 1 mm or so, where the temperature is sensed. An approximate equation for variations of brightness temperature with view angle, accurate for viewing angles $\vartheta_v \leq 75^\circ$, can be combined with an atmospheric correction algorithm originally developed for blackbody surfaces. This combined equation, which has not yet been tested, allows simultaneous corrections for atmospheric and emissivity effects from dual-channel infrared radiance measurements from satellite.

The model is also used to determine an 'all-wave' emissivity of snow for use in energy budget calculations. For all grain sizes this emissivity is between 0.985–0.990.

Acknowledgments. This work was supported by NOAA grant 00063 and CalSpace grant 18-81 to J. D. and NSF grant ATM-82-06318 to S. G. W. We appreciate comments by Sam Colbeck on liquid water in snow, and we are grateful for a thorough review by a referee.

REFERENCES

- Anderson, E. A., A point energy and mass balance model of a snow cover, *Tech. Rep. NWS 19*, 150 pp., Nat. Oceanic Atmos. Adminis., Washington, D. C., 1976.
- Anding, D., and R. Kauth, Estimation of sea surface temperature from space, *Remote Sensing Environ.*, *1*, 217–220, 1970.
- Bertie, J. E., H. J. Labbé, and E. Whalley, Absorptivity of Ice I in the range 4000–30 cm^{-1} , *J. Chem. Phys.*, *50*, 4501–4520, 1969.
- Beutner, K. J. K., and C. D. Kern, The determination of infrared emissivities of terrestrial surfaces, *J. Geophys. Res.*, *70*, 1329–1337, 1965.
- Bohren, C. F., and R. L. Beschta, Snowpack albedo and snow density, *Cold Regions Sci. Technol.*, *1*, 47–50, 1979.
- Cody, W. J., W. Fraser, and J. F. Hart, Rational Chebyshev approximation using linear equations, *Numer. Math.*, *12*, 242–251, 1968.
- Colbeck, S. C., An overview of seasonal snow metamorphism, *Rev. Geophys. Space Phys.*, *20*, 45–61, 1982.
- Deschamps, P. Y., and T. Phulpin, Atmospheric correction of infrared measurements of sea surface temperature using channels at 3.7, 11, and 12 μm , *Boundary-Layer Meteorol.*, *18*, 131–143, 1980.
- Dozier, J., A method for satellite identification of surface temperature fields of subpixel resolution, *Remote Sensing Environ.*, *11*, 221–229, 1981.
- Frampton, M. F., Measurement of snow surface temperature from thermal satellite data in the southern Sierra Nevada, Master's thesis, 51 pp., Univ. Calif., Santa Barbara, 1982.
- Gate, L. F., Light-scattering cross sections in dense colloidal suspensions of spherical particles, *J. Opt. Soc. Am.*, *63*, 312–317, 1973.
- Griggs, M., Emissivities of natural surfaces in the 8- to 14-micron spectral region, *J. Geophys. Res.*, *73*, 7545–7551, 1968.
- Hale, G. M., and M. R. Querry, Optical constants of water in the 200-nm to 200- μm wavelength region, *Appl. Opt.*, *12*, 555–563, 1973.
- Hansen, J. E., Multiple scattering of polarized light in planetary atmospheres, 2, Sunlight reflected by terrestrial water clouds, *J. Atmos. Sci.*, *28*, 1400–1426, 1971.
- Joseph, J. H., W. J. Wiscombe, and J. A. Weinman, The delta-Eddington approximation for radiative flux transfer, *J. Atmos. Sci.*, *33*, 2452–2459, 1976.
- Li, Shusun, A model for the anisotropic reflectance of pure snow, Master's thesis, Univ. Calif., 60 pp., Santa Barbara, 1982.
- McClain, E. P., Multiple atmospheric-window techniques for satellite-derived sea surface temperatures, in *Oceanography From Space*, edited by J. F. R. Gower, pp. 73–85, Plenum, New York, 1981.
- Mugnai, A., and W. J. Wiscombe, Scattering of radiation by moderately nonspherical particles, *J. Atmos. Sci.*, *37*, 1291–1307, 1980.

- Nicodemus, F. E., J. C. Richmond, J. J. Hsia, I. W. Ginsberg, and T. Limperis, Geometrical considerations and nomenclature for reflectance, *Nat. Bureau Stand. Monogr.* 160, 52 pp., 1977.
- Nussenzveig, H. M., and W. J. Wiscombe, Efficiency factors in Mie scattering, *Phys. Rev. Lett.*, 45, 1490-1494, 1980.
- Perla, R. I., and M. Martinelli, *Avalanche handbook, Handbook 489*, (rev. ed.), 254 pp., U.S. Dep. Agr., Washington, D. C., 1978.
- Pollack, J. B., and J. N. Cuzzi, Scattering by nonspherical particles of size comparable to a wavelength: a new semi-empirical theory and its application to tropospheric aerosols, *J. Atmos. Sci.*, 37, 868-881, 1980.
- Prabhakara, C., G. Dalu, and V. G. Kunde, Estimation of sea surface temperature from remote sensing in the 11- to 13- μm window region, *J. Geophys. Res.*, 79, 5039-5044, 1973.
- Reif, F., *Fundamentals of Statistical and Thermal Physics*, pp. 382-384, McGraw-Hill, New York, 1965.
- Schaaf, J. W., and D. Williams, Optical constants of ice in the infrared, *J. Opt. Soc. Am.*, 63, 726-732, 1973.
- Siegel, R., and J. R. Howell, *Thermal Radiation Heat Transfer*, 2nd ed., pp. 40-79, McGraw-Hill, New York, 1981.
- Wan, Zheng-ming, A method for digital snow mapping at subpixel resolution from NOAA thermal satellite data, Master's thesis, 46 pp., Univ. Calif., Santa Barbara, 1981.
- Warren, S. G., Optical properties of snow, *Rev. Geophys. Space Phys.*, 20, 67-89, 1982.
- Warren, S. G., and W. J. Wiscombe, A model for the spectral albedo of snow, 2, Snow containing atmospheric aerosols, *J. Atmos. Sci.*, 37, 2734-2745, 1980.
- Wiscombe, W. J., Improved Mie scattering algorithms, *Appl. Opt.*, 19, 1505-1509, 1980.
- Wiscombe, W. J., and S. G. Warren, A model for the spectral albedo of snow, 1, Pure snow, *J. Atmos. Sci.*, 37, 2712-2733, 1980.
- Zerull, R. H., R. H. Geise, S. Schwill, and K. Weiss, Scattering by particles of nonspherical shape, in *Light Scattering by Irregularly Shaped Particles*, edited by D. W. Schuerman, pp. 273-282, Plenum, New York, 1979.

(Received March 8, 1982;
revised June 27, 1982;
accepted July 14, 1982.)